doi.org/10.1002/batt.201900169

Preparation of a Self-Supported SiO_2 Membrane as a Separator for Lithium-Ion Batteries

Neil Amponsah Kyerematen,*[a, d] Dion Gukte,[b] Marc Ferch,[a] Jan Buk,[c] Tomas Hrebicek,[c] and Robert Hahn*[b]

For the first time, electrophoretic deposition (EPD) has been employed to prepare a self-supported, inorganic membrane consisting of SiO_2 nano-fibers, as a separator for lithium-ion batteries. The SiO_2 nano-fibers that were fabricated by a low-cost force spinning technique were deposited by EPD directly onto $LiNi_{0.8}Co_{0.15}Al_{0.05}O_2$ cathode material. Citric acid charging agent and anhydrous acetone solvent were used. The resulting porosity and tortuosity of the EPD SiO_2 separator were 71.42%, and 1.70, respectively. The slightly higher tortuosity of the EPD-SiO_2-fiber separator (60 μm) led to a lower rate capability in comparison to commercial GF/A glass fiber separator (260 μm). On the other hand, the latter exhibited lower self-discharge than the former in full-cells with a graphite anode; this is proposed to be related to the different purities of the two materials that impart different electronic properties or the presence of 20 wt% PVDF in the EPD-SiO_2 separator. Indeed, the deposited membrane has good characteristics as a battery separator and the EPD process is extremely feasible for the fabrication of miniaturized lithium-ion batteries on wafer level.

1. Introduction

Lithium-ion (Li-ion) batteries started to boost the marketing of portable electronic devices in 1991.[1] Owing to their high energy density and efficiency, they have now instigated the mass commercialization of electric vehicles with good autonomy.[2] Miniaturized forms of Li-ion batteries have also been successfully adopted for micro-electronic applications.[3] The great success of the Li-ion technology achieved, so far, is because of the significant research and development efforts dedicated to it since the past three decades.[4] However, Li-ion batteries truly perform far below their theoretical capabilities. It is still believed that the performance of Li-ion or lithium-based batteries can be drastically improved if significant progress is made in electrode and electrolyte materials.[5]

Apart from the focus on electrode and electrolyte materials, various approaches are also being investigated to develop better separator materials for Li-ion batteries.[6] Actually, separators account for about 20% of the Li-ion battery cost, and much of that cost relates to the separator's production alone; hence, there is still significant interest in cost-effective fabrication methods for Li-ion battery separators.[7] The separator is an indispensable component of the Li-ion battery as it prevents direct contact between the anode and cathode of the cells to minimize self-discharge. It also ensures effective transport of electro-active species (i.e. lithium ions) from one electrode to another via the absorbed electrolyte. Conventionally, polyolefins, especially polypropylene materials (Celgard®) are used as the separator for commercial Li-ion batteries.[1b,8] The principal requirements of a battery separator include (*i*) good chemical and electrochemical stability, (*ii*) good porosity, (*iii*) high electrical resistance, (*iv*) good wettability, (*v*) good thermal stability and (*vi*) good mechanical strength. Though the Celgard® separators sufficiently meet most of the above requirements, their polymeric nature undermines their thermal and mechanical stabilities which are very necessary for overcoming the thermal runaway issues of Li-ion batteries.

In fact, tri-layered polyolefin separators, consisting of a polyethylene (PE) layer sandwiched between two polypropylene (PP) layers, exhibit the "shut-down" effect: that is in case of overheating, the PE layer melts, losing its porosity and mechanically blocking Li^+ ion movement (to shut down the cell, and avoid thermal runaway); though the PP layer can prevent some dimensional changes, it will also eventually melt.[6a,7a,9] Thus, such polymeric separators have a serious thermal limitation: either significant shrinkage at 100 °C, or definite irreversible melting at $T \geq 135$ °C).[6a,9] Although composite separators with polymers and inorganic particles offer excellent wettability and better thermal stability simultaneously, they are not mechanically well-adapted to withstand handling in cell winding and assembly.[6e,7a,10] As a consequence, bi-layer separators called Separion® which consist of polymeric

[a] Dr. N. A. Kyerematen, M. Ferch
Micro Energy Storage Group, Research Center for Microperipheric Technologies, Technical University of Berlin, 13355 Berlin, Germany
[b] D. Gukte, Dr. R. Hahn
Fraunhofer Institut für Zuverlässigkeit und Mikrointegration (IZM), Micro Energy Storage Group, 13355 Berlin, Germany
E-mail: Robert.hahn@izm.fraunhofer.de
[c] J. Buk, T. Hrebicek
Pardam, Žižkova 2759, 413 01, Roudnice nad Labem, Czech Republic
[d] Dr. N. A. Kyerematen
Center for Process Innovation (CPI), Nanomaterials and Composites, The Coxon Building, John Walker Road, Sedgefield, County Durham, TS21 3FE, England, United Kingdom
Fax: +49 3046403-123
E-mail: amponsah.kyerematen@uk-cpi.com

non-woven mats coated with a thin layer of inorganic (SiO_2, CeO_2, Al_2O_3, ZrO_2 etc.) nano-particles have also emerged.[7a] The Separion® performs better than all the aforementioned separator types as the polyethylene terephthalate (PET) mat – which has a high melting point of 260 °C – imparts better thermal stability, and the anchored inorganic nanoparticles also impart better mechanical properties; it is thus receiving attention for cells for automotive applications.[11]

Recently, much attention is being given to free-standing, inorganic separators consisting mostly of SiO_2, CeO_2, Al_2O_3, or ZrO_2 and being engineered for flexibility to withstand winding.[6d,12] Shi *et al.*[6b] have succeeded to prepare a flexible, free-standing, polymer-free, inorganic separator based on SiO_2 fibers; the polymeric content was removed via a thermal treatment in air. He *et al.*[13] have also prepared a free-standing, inorganic separator based on Al_2O_3 nano-wires without using any polymer additives. Indeed, the traditional insulating inorganic materials can be exploited to develop better separators for safer Li-ion batteries; however, significant advances in processing methods are still required. Furthermore, as demonstrated by Honma and co-workers,[14] the traditional, insulating inorganic materials can even be exploited to develop free-standing quasi-solid-state electrolytes for bi-polar lithium batteries.

Although the free-standing inorganic separators are good, for some applications (especially those requiring miniaturized Li-ion batteries), it will be ideal to fabricate the separator as a self-supported layer on one electrode; that can even allow to fabricate much thinner separators, for instance, for wafer-level fabrication of Li-ion micro-batteries.[15] In this work, electrophoretic deposition (EPD) was investigated – for the first time – as a cost-effective method for preparing a self-supported inorganic membrane, consisting of SiO_2 nano-fibers, as a separator for Li-ion batteries. Physico-chemical characterization of the obtained membrane has been done. A thorough electrochemical characterization has also been done to fully evaluate the suitability of the membrane as a separator for Li-ion batteries.

Experimental Section

Electrode preparation

$LiNi_{0.8}Co_{0.15}Al_{0.05}O_2$ (NCA), purchased from Toda, was mixed with C65 carbon black and PVDF binder in the ratio of 92:4:4 wt% in NMP solvent. A homogeneous slurry (agglomerate size below 25 μm) was achieved by processing several times in the mixer (SpeedMixer™ DAC 150 SP) in combination with ultrasonic treatment (ultrasonic sonotrode UP2000ST, Hielscher Ultrasonics GmbH). The cathode film was then made by tape casting with TQC (AB3220) automatic film applicator.

Production of SiO_2 nanofibers

Highly, cost-efficient, force spinning was used for the production of SiO_2 nanofibers. Pardam has developed SiO_2 nanofibers from a new precursor, which is thousand-fold cheaper than TEOS, normally used for production of inorganic nanofibers. An industrial line Cyclone TOWER was used for the fiber production. Ethanol that is typically used has been replaced by water in the solution system, so the whole process is much cheaper and characterized by higher yield. After spinning, calcination was done in an industrial calcination furnace and, finally, ball milling was used to shorten the fiber length to ca. 40 μm. The milling was required to facilitate the stability of the fibers in the EPD suspension.

Electrophoretic deposition

The suspension for the EPD consisted of milled SiO_2 nanofibers (1 g/l), citric acid (0.2 g/l) and PVDF (0.4 g/l) using acetone as solvent. Stirring and sonication were alternated to achieve a very stable suspension. The acetone was dried with molecular sieves for 2 days before use. A constant potential EPD was carried out with an electric field of 50 V/cm, with the cathode film as the working electrode, and a stainless plate as the counter electrode.

Physico-chemical characterization

Scanning electron microscopy (SEM) was done using a Zeiss Leo 1530 scanning electron microscopy. For cross-section, the samples were cut with scissors; for observing the GF/A separator, Pt was sputtered (for 30s) onto the separator.

Electrochemical measurements

All electrochemical experiments were done with PAT cells in a climatic chamber at a constant temperature of 25 °C. Half-cells and full-cells were assembled with GF/A glass fiber separator soaked with LP30 electrolyte (1 M $LiPF_6$ in EC:DMC 1:1 vol. UBE). Cell testing was done employing a Basytec CTS-XL multichannel battery tester. The cut-off voltages for the half-cells and full cells were $3.0 \leq U(V \text{ vs } Li/Li^+) \leq 4.2$ and $3.0 \leq U(V) \leq 4.1$, respectively, with a CC-CV program consisting of charge at 0.1 C and discharge at variable currents.

2. Results and Discussion

2.1. Morphology and Composition

Electrophoretic deposition is a simple, versatile, scalable and relatively inexpensive route for preparing thick films; and it requires only an electric field and a suspension of charged particles.[16] EPD is receiving significant attention, recently, for the processing of battery[17] and supercapacitor[18] materials. The main challenge of the EPD process is the difficulty in choosing the right charging agent for a stable suspension.[16b,19] Citric acid was chosen as the charging agent for this work; it has been previously reported as a good charging agent with acetone solvent for EPD.[20] Indeed, the combination of the citric acid charging agent and the ball-milled SiO_2 nano-fibers (diameter: 100–300 nm, length: 2–40 μm) gave a stable suspension in acetone. Zeta potential (ζ) of −10 mV was measured with *Zetasizer nanoseries* from Malvern Instruments; the charge on the fibers is probably higher than it was measured, considering that the technique is mostly suitable for spherical particles. Moreover, a BET surface area of 97 m^2/g was measured for the starting SiO_2 powder, confirming the high

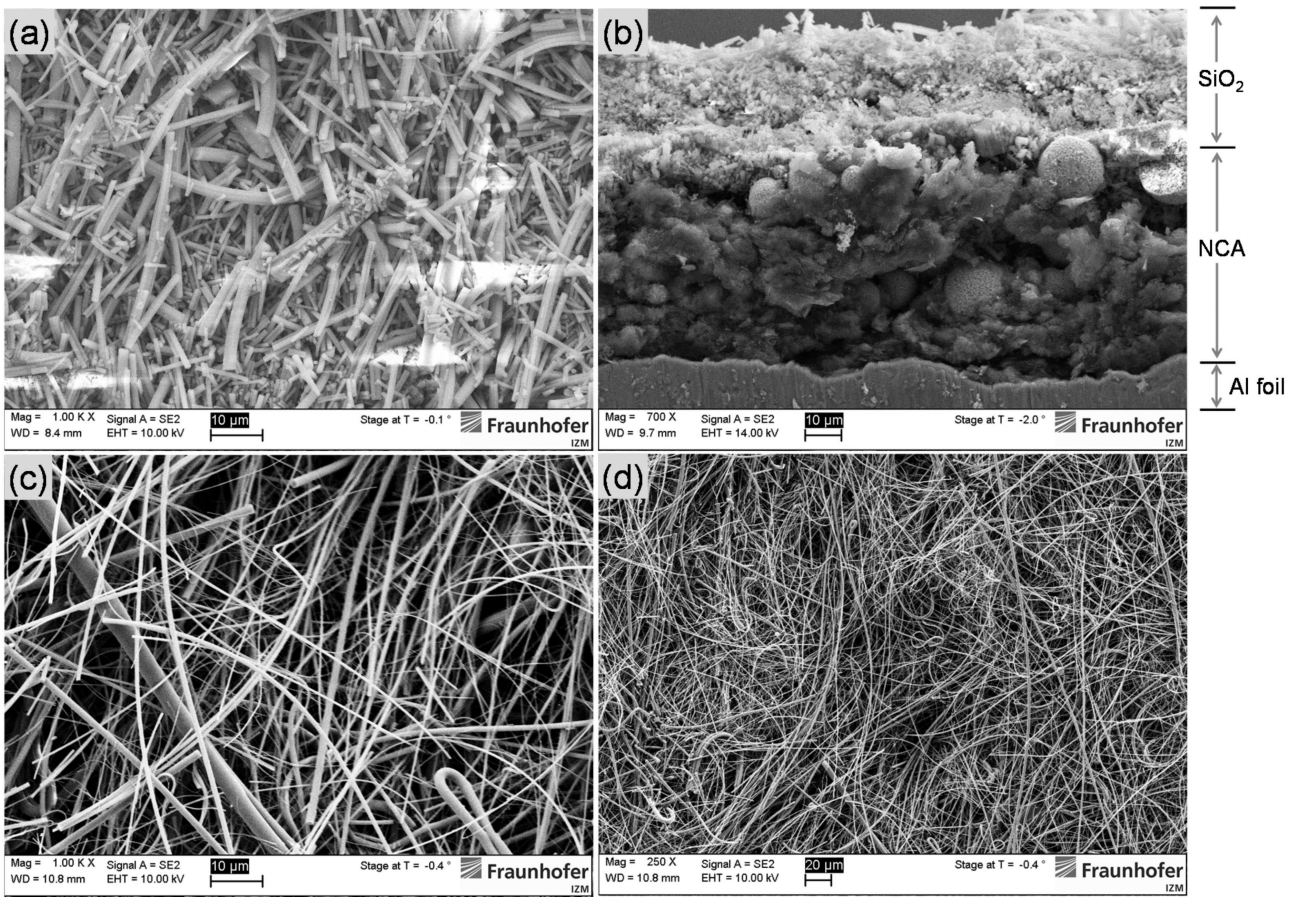

Figure 1. SEM images of (a–b) EPD SiO_2 membrane deposited onto $LiNi_{0.8}Co_{0.15}Al_{0.05}O_2$ (NCA) electrode (in top-view and cross-section), and (c–d) GF/A glass fiber separator at different magnifications.

surface area of the nanostructured material. Citric acid, as a weak acid, gets ionized upon dissolution in acetone according to the reaction given in Eq. (1); and the anion is adsorbed around the SiO_2 nano-fibers. This is consistent with the negative zeta potential measured.

$$C_6H_8O_7 \rightarrow C_6H_5O_7^{3-} + 3H^+ \quad (1)$$

The constant potential EPD gave very uniform thick films of SiO_2 nano-fibers on $LiNi_{0.8}Co_{0.15}Al_{0.05}O_2$ (NCA) cathode (ca. 70 μm thick) prepared beforehand by tape casting. Representative cross-sectional and top-view SEM images of the deposited SiO_2 are presented in Figure 1, together with the surface view of a commercially available GF/A glass fiber separator at different magnifications. It is worth emphasizing that the solvent and charging-agent system used was very effective as very homogeneous films were obtained with the constant electric field EPD, without the need for pulse-field EPD. The evolution of deposited SiO_2 thickness with deposition time, as well as deposited mass with thickness is showcased in Figure 2; it can be noticed from Figure 2a that, as expected, a direct linear relationship exists for the deposition time and thickness until $t = 15$ min – this is in agreement with the deviation from Hamaker's law, as a consequence of the reduction of the electric field strength during the deposition as a thick insulating SiO_2 layer is grown on the electrode's surface. The elemental analysis (energy dispersive spectroscopy) results obtained for the starting powder and the EPD materials are shown in Table 1. From the EDS results, the fluorine proportion was estimated to be approx. 21 % of the Si content, which is in good agreement with the initial PVDF proportion (20 wt % with respect to the SiO_2 powder) added to the suspension. Moreover, a very small contamination (1 at %) of sodium was identified in the starting powder and in the EPD layer; this contamination comes from the precursor of the water/glass colloid suspension used to produce the SiO_2 nano-fibers.

No other metallic impurities were identified, which is an indication of the high-quality of the ball milling tools used to

Table 1. EDS elemental analysis of starting SiO_2 powder and EPD deposited SiO_2.

Element	Powder SiO_2 at %	EPD SiO_2 at %
Si	36.36	27.25
Na	1.0	0.6
O	57.25	50.5
C	5.39	15.68
F	0	5.97

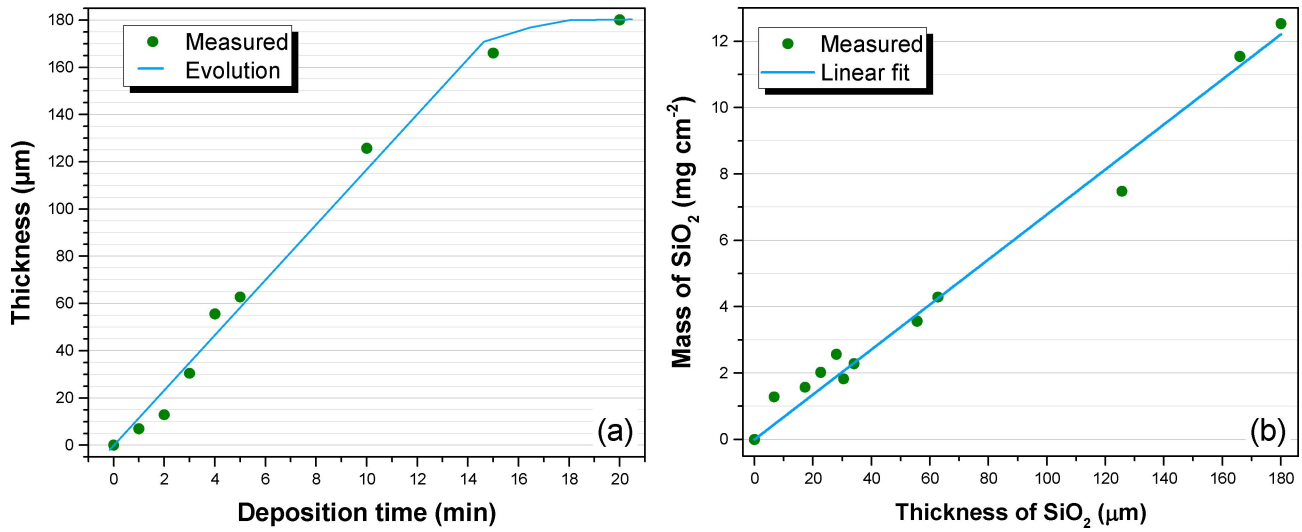

Figure 2. Evolution of deposition time with deposited SiO_2 thickness (a), and deposited mass with thickness (b).

shorten the lengths of the fibers. While the small carbon proportion (5.39 at%) in the powder sample is actually emanating from the carbon tape used for the SEM, the higher amount (15.68 at%) of carbon in the EPD SiO_2 can be ascribed to the binder in the deposited layer, considering that the EPD SiO_2 layer is deposited on the cathode material. Actually, the EDS of the EPD SiO_2 was done on the surface of a sample with a thick EPD SiO_2 layer, to avoid any signal from the underlying cathode composite.

Furthermore, it was imperative to determine the porosity of the SiO_2 membrane made by EPD in order to properly benchmark its electrochemical performance. The porosity (ε) of the membrane was estimated to be 71.42% using the relation given in Eq. 2; where ρ_b corresponds to the bulk density of the membrane – which is defined by its apparent mass and volume ($\rho_b = 0.69$ g/cm^3) –, and ρ_p corresponds to the particle density of the material. As SEM revealed that the binder content in the suspension was kept in the deposit, the particle density of the membrane was estimated to be 2.414 g/cm^3 considering a composite comprising 20 wt% PVDF ($\rho = 1.78$ g/cm^3) and 80 wt% SiO_2 ($\rho = 2.65$ g/cm^3), and using the relation given in Eq. (3); where ρ_c is the density of the composite EPD-SiO_2 separator, and w_i and ρ_i correspond to the weight fraction and density of the components, respectively. Indeed, the relation given in Eq. (2) is well reported to give reasonable values of porosity.[6e] Moreover, a porosity of 92.2% was estimated for the GF/A glass fiber separator (please see Figure 1c–d) which is very consistent with the experimental porosity (91%) provided by the supplier. Thus, the GF/A glass fiber separator is more porous than the EPD-SiO_2 separator, which is significantly obvious from the morphology shown in the SEM images of Figure 1.

$$\varepsilon = \left(1 - \frac{\rho_b}{\rho_p}\right) \times 100\,\% \qquad (2)$$

$$\rho_c = \left(\frac{1}{\frac{w_1}{\rho_1} + \frac{w_2}{\rho_2}}\right) \times 100\,\% \qquad (3)$$

2.2. Electrochemical Performance

The performance of the EPD SiO_2, self-supported on $LiNi_{0.8}Co_{0.15}Al_{0.05}O_2$ (NCA) was evaluated as a separator for lithium-ion batteries in comparison to a commercially available GF/A glass fiber separator. The voltage profiles of the galvanostatic cycling performance of the NCA half-cell with only GF/A glass fiber separator is presented in Figure 3a; the first discharge capacity was 168 mAh/g at 0.1 C, and it did not fade for up to 50 charge/discharge cycles. It can be noted that the charge is always followed by a short potential plateau due to the constant current-constant potential (CC-CV) program used to cycle the cells.

The rate capability of NCA half-cell with only GF/A glass fiber separator is presented in Figure 3b together with those of NCA electrodes coated with EPD-SiO_2 layers of different thicknesses. Due to the use of lithium counter electrode, the NCA electrodes coated with EPD-SiO_2 were additionally covered with two GF/A glass fiber separators (each of 260 μm) as was done for the non-coated electrodes. Actually, without the GF/A glass fiber separators, the half cells could not be properly charged due to the formation of dendrites. It can be noted from Figure 3b that the rate capability is nearly the same from 0.1 C to 3 C, but from 3 C to 10 C, the rate capability decreases with increasing SiO_2 layer thickness; this is consistent with pronounced diffusion limitation as a consequence of increased ionic transport length for the charge/discharge reactions.

Furthermore, the effect of the EPD process on the performance of the NCA cathode in full-cells with graphite anode was evaluated by measuring the discharge capacities of electrodes with varying EPD SiO_2 separator thickness on the cathode. As

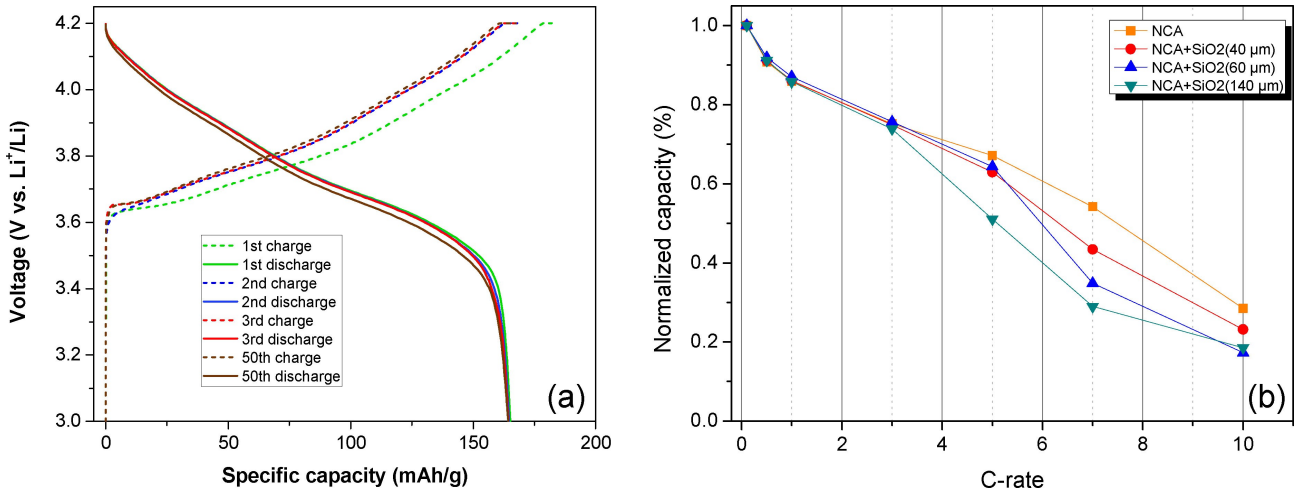

Figure 3. Charge/discharge voltage profile of NCA half-cell with a 520 µm GF/A glass fiber separator (a); effect of the presence of EPD-SiO_2 on the rate capability of NCA half-cells with GF/A glass fiber separator (b).

shown in Figure 4a, the discharge capacity after formation (at 0.1 C) is higher with the GF/A glass fiber separator (no EPD process), and it decreases quite linearly with increasing EPD-SiO_2 separator thickness or increasing deposition time. Though

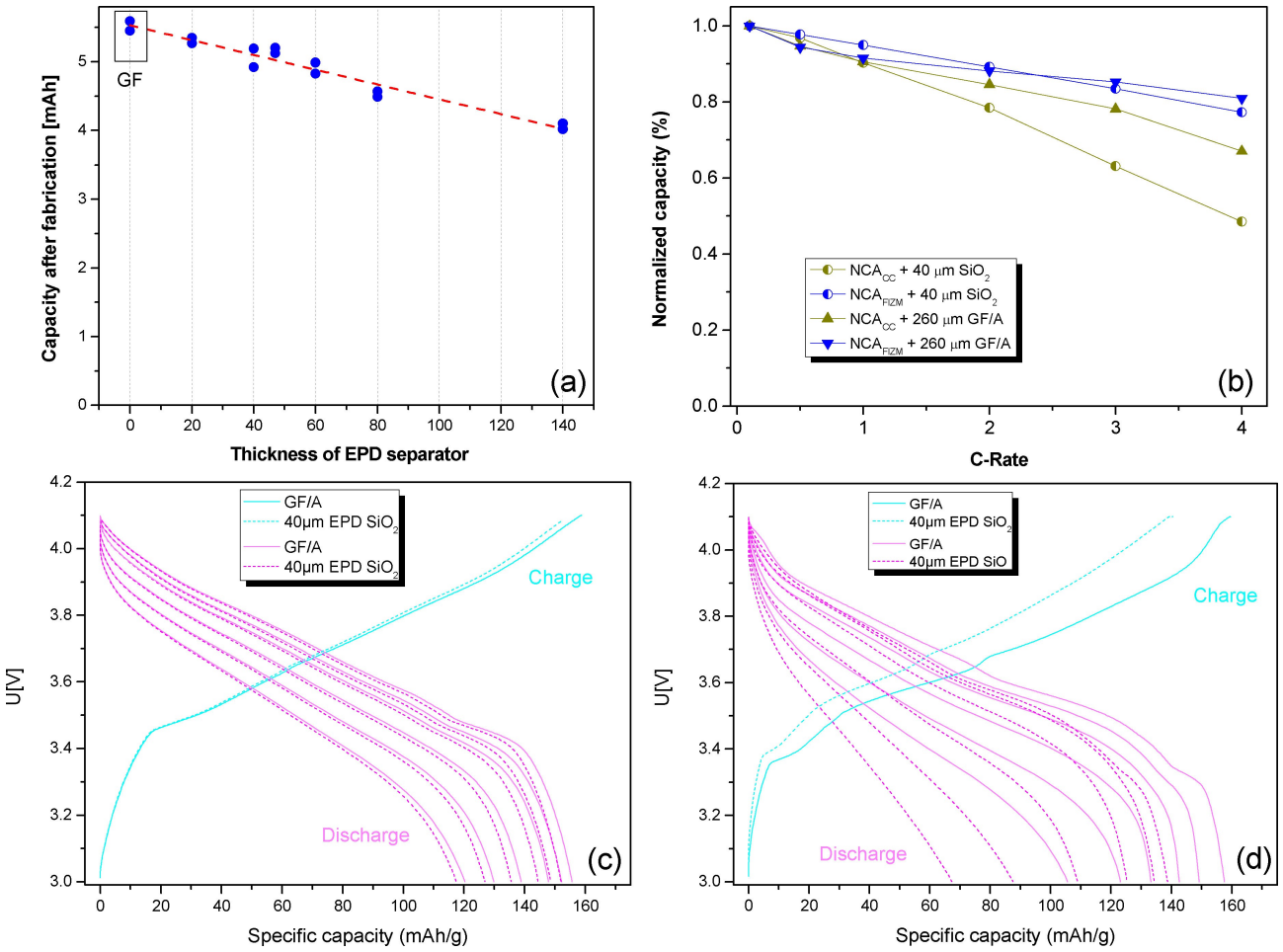

Figure 4. Effect of the EPD process on the attainable capacity of NCA full cells at 0.1 C (a), and rate capability of NCA/ graphite full cells (NCA_{FIZM}: made in-house; NCA_{cc}: purchased from custom cells) with 40 µm EPD-SiO_2 or 260 µm GF/A glass fiber separator (b). Voltage profiles of the NCA_{FIZM}/graphite (c) and NCA_{cc}/graphite (d) full-cells at different discharge rates.

40, 60, and 140 μm were the main thicknesses studied, 20, 47 and 80 μm films were made to verify the observed trend. The employed acetone was dried, but it might have still absorbed some moisture during the deposition or it can just be direct humidity interaction with the cathode material that caused some lithium leach-out. It is also suspected that the applied deposition voltage (50 V) might induce some structural changes in the material or exacerbate the lithium leach-out in the humid environment. As the 40 μm EPD-SiO_2 membrane gave the best rate capability in half-cells than the 60 and 140 μm membranes, that thickness was chosen for the subsequent electrochemical studies.

What is more, the effect of EPD-SiO_2 on the rate capability of NCA-graphite full-cells without any GF/A glass fiber separator is presented in Figure 4b. It can be noticed that irrespective of the NCA cathode material type (one made in-house, as described, and another commercial) the thinner EPD-SiO_2 separator (40 μm) imparts pronounced poor rate capability (especially from 3 C) to the full-cell in comparison to the GF/A glass fiber separator. This behavior is in agreement with the trend observed in the half-cells of Figure 3b, and it can be related to the different tortuosities of the EPD SiO_2 and the GF/A glass fiber separators. Also, the voltage profiles of the full-cells at varied discharge rates are presented in Figure 4c–d. It can be noticed that the commercial cathode (NCA_{cc}) shows much polarization and poorer rate capability as it is thicker, and significantly calendared.

The tortuosities (τ) of the EPD SiO_2 (40 μm) and the GF/A glass fiber (260 μm) were estimated to be 1.70 and 1.38, respectively, using the relation given in Eq. (4);[8] where ε is the porosity, R_e is the electrolyte resistance determined from the ionic conductivity of the electrolyte (11.19×10^{-3} S cm^{-1}) and the cell constant of each separator, and R_s is the resistance of each separator material placed between 2 stainless steel plates and soaked with liquid electrolyte in the PAT cell. The R_s resistances were determined with the help of electrochemical impedance spectroscopy. For this purpose, EPD of the SiO_2 was done on a stainless steel plate, whilst the glass fiber separator was just sandwiched between two stainless steel foils. The tortuosities of the two materials are consistent with their morphologies; according to literature, $\tau > 1$ is indicative of a hindered system which consists of non-cylindrical and non-parallel pores.[6a] The poor rate capability of the EPD SiO_2-based full-cells, in comparison to the GF/A glass fiber separator, can indeed be corroborated by its higher tortuosity and lower porosity.

$$\tau = \sqrt{\frac{R_s}{R_e} \times \varepsilon} \tag{4}$$

Furthermore, to characterize the effectiveness of the EPD-SiO_2 as a separator material for LIBs, the self-discharge of the Graphite/NCA full-cell with the EPD-SiO_2 separator was estimated and compared to that of a GF/A separator. To achieve that, after the formation at 0.1 C, one galvanostatic charge/discharge cycle followed by one charge at 0.1 C were done, and the state-of-charge (at open circuit potential) was subsequently monitored for 336 hrs (14 days) followed by two galvanostatic discharge/charge cycles, as showcased in Figure 5a. Consequently, as shown in Figure 5b, the self-discharge (SD) of the graphite/NCA cells with EPD-SiO_2 or GF/A separator were estimated to be 6.0% and 7.4%, respectively, using the relation given in Eq. (5).[21] As shown in Figure 5a, the open-circuit-potential drop during the storage was more with the GF/A separator cell than with the EPD-SiO_2 separator cell. It can thus be asserted that the GF/A separator has some impurities that cause the potential drop during the storage, and consequently, the slightly higher self-discharge or it is the presence of the 20 wt% PVDF binder that improves the self-discharge characteristics of the much thinner EPD-SiO_2 separator.

$$\mathrm{SD} = \frac{(D_1 - D_2)}{D_1} \times 100\,\% \tag{5}$$

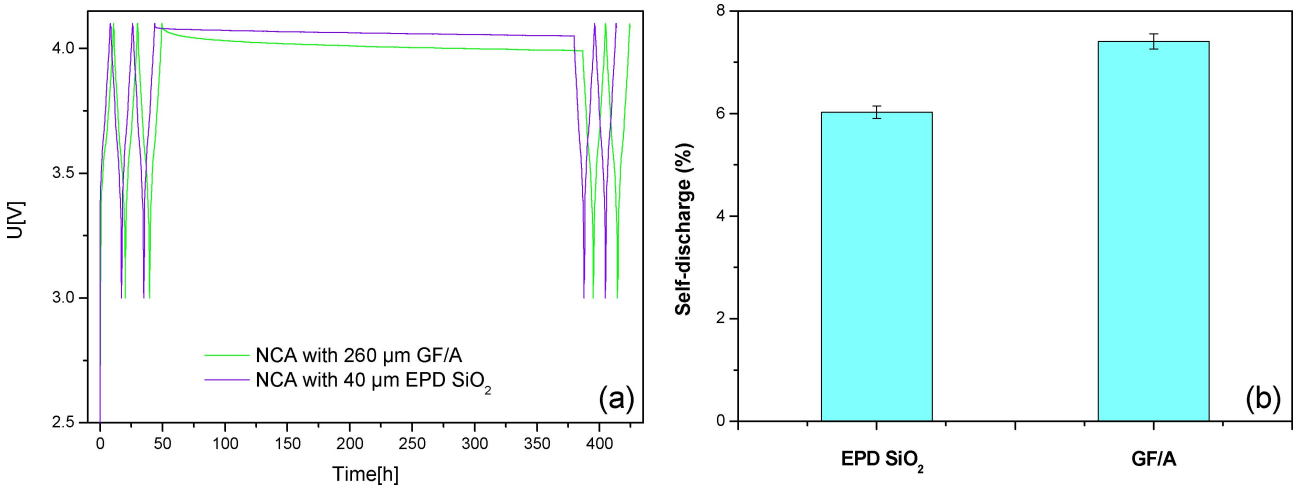

Figure 5. Comparison of (a) voltage profiles of galvanostatic cycling with 14 days state-of-charge evolution, and (b) estimated self-discharge, for Graphite/NCA full-cell with GF/A or EPD-SiO_2 separators.

Where D_1 corresponds to the last discharge capacity before storage, and D_2 corresponds to the discharge capacity directly after storage.

3. Conclusions

The suitability of electrophoretic deposition (EPD) to prepare self-supported SiO_2 as a separator membrane for Li-ion batteries has been demonstrated. The EPD separator made with SiO_2 nanofibers is less porous and more tortuous than commercial GF/A glassfiber separator; this led to poor rate capability in full cells with the former even though it was much thinner. However, the thinner EPD-SiO_2 separator exhibited lower self-discharge than the thicker GF/A glassfiber separator – which is believed to be more related to the presence of 20 wt% PVDF in the EPD-SiO_2 separator. The proposed method cannot only be extremely useful for preparing self-supported separator membranes for miniaturized LIBs with liquid electrolytes, but also for all-solid-state batteries where the self-standing SiO_2 membrane can be infiltrated with a solution of a soluble sulphide solid-state electrolyte and dried – as demonstrated by Kim et al.[22] Future works will be aimed at determining the experimental conditions that are causing the NCA cathode electrodes subjected to the EPD process to deliver lower capacities than those not subjected to EPD but directly tested with the GF/A separator. Additional works will also investigate EPD of the SiO_2 separator onto anode materials such as graphite and $Li_4Ti_5O_{12}$.

Acknowledgements

We are grateful to Karla Kern and Denis Bernsmeier of TU Berlin for the Zeta potential and BET measurements, respectively. This work was supported by the BMBF hearing-aid battery project (Project #: 10043013). Open access funding enabled and organized by Projekt DEAL.

Conflict of Interest

The authors declare no conflict of interest.

Keywords: electrophoretic deposition · silica nanofibers · separator · batteries · energy storage

[1] a) J. M. Tarascon, M. Armand, *Nature* **2001**, *414*, 359–367; b) M. Yoshio, R. J. Brodd, B. Kozawa, *Lithium-Ion Batteries: Science and Technologies*, Springer, New York, NY, **2009**.
[2] D. Larcher, J. M. Tarascon, *Nat. Chem.* **2015**, *7*, 19–29.
[3] a) N. A. Kyeremateng, *ChemElectroChem* **2014**, *1*, 1442–1466; b) N. A. Kyeremateng, R. Hahn, *ACS Energy Lett.* **2018**, *3*, 1172–1175.
[4] J. Janek, W. G. Zeier, *Nat. Energy* **2016**, *1*, 16141.
[5] a) H. Zhou, H. Cheng, H. Zhao, K. Zhao, Y. Zhao, J. Zhang, Q. Xu, X. Lu, *J. Electrochem. Soc.* **2019**, *166*, A59–A67; b) X. Zhang, Y. Fan, M. A. Khan, H. Zhao, D. Ye, J. Wang, B. Yue, J. Fang, J. Xu, L. Zhang, J. Zhang, *Batteries & Supercaps*, **2020**, *3*, 108–116; c) N. Nitta, F. Wu, J. T. Lee, G. Yushin, *Mater. Today* **2015**, *18*, 252–264; d) P. Rozier, J. M. Tarascon, *J. Electrochem. Soc.* **2015**, *162*, A2490–A2499; e) L. Wen, J. Liang, J. Chen, Z.-Y. Chu, H.-M. Cheng, F. Li, *Small Methods* **2019**, *3*, 1900323.
[6] a) P. Arora, Z. Zhang, *Chem. Rev.* **2004**, *104*, 4419–4462; b) C. Shi, J. Zhu, X. Shen, F. Chen, F. Ning, H. Zhang, Y.-Z. Long, X. Ning, J. Zhao, *RSC Adv.* **2018**, *8*, 4072–4077; c) M. Kirchhöfer, J. von Zamory, E. Paillard, S. Passerini, *Int. J. Mol. Sci.* **2014**, *15*, 14868–14890; d) X. Yinyu, L. Junsheng, L. Jiaheng, L. Dan, X. Zhizhong, Q. Deyu, L. Ke, D. Tengfei, T. Haolin, *ChemSusChem* **2016**, *9*, 3023–3039; e) H. Lee, M. Yanilmaz, O. Toprakci, K. Fu, X. Zhang, *Energy Environ. Sci.* **2014**, *7*, 3857–3886; f) M. F. Lagadec, R. Zahn, V. Wood, *Nat. Energy* **2019**, *4*, 16–25; g) J. Moon, J. Y. Jeong, J. I. Kim, S. Kim, J. H. Park, *J. Power Sources* **2019**, *416*, 89–94; h) C. M. Costa, Y.-H. Lee, J.-H. Kim, S.-Y. Lee, S. Lanceros-Méndez, *Energy Storage Mater.* **2019**, *22*, 346–375; i) X. Yuan, H. Liu, J. Zhang, *Lithium-Ion Batteries: Advanced Materials and Technologies*, CRC Press, **2016**.
[7] a) S. S. Zhang, *J. Power Sources* **2007**, *164*, 351–364; b) V. Deimede, C. Elmasides, *Energy Technol.* **2015**, *3*, 453–468.
[8] X. Huang, *J. Solid State Electrochem.* **2011**, *15*, 649–662.
[9] G. Venugopal, J. Moore, J. Howard, S. Pendalwar, *J. Power Sources* **1999**, *77*, 34–41.
[10] Y. Xiang, J. Li, J. Lei, D. Liu, Z. Xie, D. Qu, K. Li, T. Deng, H. Tang, *ChemSusChem* **2016**, *9*, 3023–3039.
[11] Evonik, *Vol. 2019*.
[12] D. Carvalho, N. Loeffler, G.-T. Kim, S. Passerini, *Membranes* **2015**, *5*, 632.
[13] M. He, X. Zhang, K. Jiang, J. Wang, Y. Wang, *ACS Appl. Mater. Interfaces* **2015**, *7*, 738–742.
[14] a) Y. Gambe, Y. Sun, I. Honma, *Sci. Rep.* **2015**, *5*; b) T. Matsuo, Y. Gambe, Y. Sun, I. Honma, *Sci. Rep.* **2014**, *4*, 6084.
[15] R. Hahn, M. Ferch, K. Tribowski, N. A. Kyeremateng, K. Hoeppner, K. Marquardt, K.-D. Lang, W. Bock, *Microsyst. Technol.* **2019**, *25*, 1137–1149.
[16] a) N. A. Kyeremateng, D. Ty Mai, D. Pech, *RSC Adv.* **2015**, *5*, 61502–61507; b) L. Besra, M. Liu, *Prog. Mater. Sci.* **2007**, *52*, 1–61.
[17] a) C. C. Lalau, C. T. J. Low, *Batteries & Supercaps* **2019**, *2*, 551–559; Supercaps **2019**, 2, 551–559; b) L. Ye, K. Wen, Z. Zhang, F. Yang, Y. Liang, W. Lv, Y. Lin, J. Gu, J. H. Dickerson, W. He, *Adv. Energy Mater.* **2016**, *6*, 1502018; c) M. Uceda, J. Zhou, J. Wang, R. Gauvin, K. Zaghib, G. P. Demopoulos, *Electrochim. Acta* **2019**, *299*, 107–115; d) B. Gangaja, H. P. Muralidharan, S. Nair, D. Santhanagopalan, *ACS Sustainable Chem. Eng.* **2018**, *6*, 4705–4710.
[18] a) N. A. Kyeremateng, T. Brousse, D. Pech, *Nat. Nanotechnol.* **2017**, *12*, 7–15; b) D. Pech, M. Brunet, H. Durou, P. Huang, V. Mochalin, Y. Gogotsi, P.-L. Taberna, P. Simon, *Nat. Nanotechnol.* **2010**, *5*, 651–654.
[19] a) I. Corni, M. P. Ryan, A. R. Boccaccini, *J. Eur. Ceram. Soc.* **2008**, *28*, 1353–1367; b) M. Ammam, *RSC Adv.* **2012**, *2*, 7633–7646; c) M. S. Ata, Y. Liu, I. Zhitomirsky, *RSC Adv.* **2014**, *4*, 22716–22732.
[20] A. Caballero, L. Hernan, M. Melero, J. Morales, R. Moreno, B. Ferrari, *J. Power Sources* **2006**, *158*, 583–590.
[21] E. Redondo-Iglesias, P. Venet, S. Pelissier, in *VPPC*, Hangzhou, China, **2016**.
[22] D. H. Kim, D. Y. Oh, K. H. Park, Y. E. Choi, Y. J. Nam, H. A. Lee, S.-M. Lee, Y. S. Jung, *Nano Lett.* **2017**, *17*, 3013–3020.

Manuscript received: November 2, 2019
Revised manuscript received: November 24, 2019
Accepted manuscript online: December 9, 2019
Version of record online: February 3, 2020